

PROCEEDINGS OF SPIE

[SPIDigitalLibrary.org/conference-proceedings-of-spie](https://spiedigitallibrary.org/conference-proceedings-of-spie)

NIP: the near infrared imaging photometer for Euclid

Mario Schweitzer, Ralf Bender, Reinhard Katterloher, Frank Eisenhauer, Reiner Hofmann, et al.

Mario Schweitzer, Ralf Bender, Reinhard Katterloher, Frank Eisenhauer, Reiner Hofmann, Roberto Saglia, Rory Holmes, Oliver Krause, Hans-Walter Rix, Jeff Booth, Parker Fagrelus, Jason Rhodes, Suresh Seshadri, Alexandre Refregier, Jerome Amiaux, Jean-Louis Augueres, Olivier Boulade, Christophe Cara, Adam Amara, Simon Lilly, Eli Atad-Ettinger, Anna-Maria Di Giorgio, Ludovic Duvet, Christopher Kuehl, Mohsin Syed, "NIP: the near infrared imaging photometer for Euclid," Proc. SPIE 7731, Space Telescopes and Instrumentation 2010: Optical, Infrared, and Millimeter Wave, 77311K (5 August 2010); doi: 10.1117/12.857031

SPIE.

Event: SPIE Astronomical Telescopes + Instrumentation, 2010, San Diego, California, United States

NIP - The Near Infrared Imaging Photometer for Euclid

^aMario Schweitzer, ^aRalf Bender, ^aReinhard Katterloher, ^aFrank Eisenhauer, ^aReiner Hofmann, ^aRoberto Saglia, ^bRory Holmes, ^bOliver Krause, ^bHans-Walter Rix, ^cJeff Booth, ^cParker Fagrelus, ^cJason Rhodes, ^cSuresh Seshadri, ^dAlexandre Refregier, ^dJerome Amiaux, ^dJean-Louis Augueres, ^dOlivier Boulade, ^dChristophe Cara, ^eAdam Amara, ^eSimon Lilly, ^fEli Atad-Ettedgui, ^gAnna-Maria Di Giorgio, ^hLudovic Duvet, ⁱChristopher Kuehl, ⁱMohsin Syed

^aMax-Planck-Institute for Extraterrestrial Physics, Garching, Germany

^bMax-Planck-Institute for Astronomy, Heidelberg, Germany

^cJet Propulsion Laboratory, Pasadena, United States

^dService d'Astrophysique CEA, Saclay, France

^eETH Department of Physics, Zurich, Switzerland

^fRoyal Observatory, Edinburgh, United Kingdom

^gIFSI-INAF, Rome, Italy

^hESTEC, Noordwijk, Netherlands

ⁱEADS, Astrium Satellites, Munich, Germany

ABSTRACT

The NIP is a near infrared imaging photometer that is currently under investigation for the *Euclid* space mission in context of ESA's 2015 Cosmic Vision program. Together with the visible camera (VIS) it will form the basis of the weak lensing measurements for *Euclid*. The NIP channel will perform photometric imaging in 3 near infrared bands (Y, J, H) covering a wavelength range from ~ 0.9 to $2 \mu\text{m}$ over a field of view (FoV) of $\sim 0.5 \text{ deg}^2$. With the required limiting point source magnitude of 24 mAB (5 sigma) the NIP channel will be used to determine the photometric redshifts of over 2 billion galaxies collected over a wide survey area of $20\,000 \text{ deg}^2$. In addition to the photometric measurements, the NIP channel will deliver unique near infrared (NIR) imaging data over the entire extragalactic sky, enabling a wide variety of ancillary astrophysical and cosmological studies. In this paper we will present the results of the study carried out by the *Euclid* Imaging Consortium (EIC) during the *Euclid* assessment phase.

Keywords: Euclid, NIP, Near Infrared Photometer, Photometric Redshifts

1. INTRODUCTION

Euclid is a candidate mission for ESA's Cosmic Vision program. Its purpose is to map the geometry and evolution of the dark universe with unprecedented precision. Its primary goal is to place high accuracy constraints on dark energy, dark matter, gravity and cosmic initial conditions using two independent cosmological probes: weak gravitational lensing and baryonic acoustic oscillations. For this purpose, *Euclid* will measure the shapes and redshifts of more than 2 billion galaxies over the entire extragalactic sky in the visible and near infrared, out to redshift ~ 2 , thus covering the period over which dark energy accelerated the expansion of the universe. The measured photometric redshifts will reach a precision of $\frac{\sigma(z)}{1+z} = 0.03 - 0.05$. They will be derived using three near infrared filters (Y,J,H in the range $\sim 0.9 - 2.0 \mu\text{m}$) located in the NIP channel. To achieve the required photometric precision the NIP data will be complemented by ground based photometry in multiple visible bands. Beside *Euclid*'s cosmology primary science case the NIP channel will further produce extensive legacy science data for various fields of astronomy .

This paper discusses NIP, the Near Infrared Imaging Photometer on *Euclid*, as envisaged at the end of the assessment phase. The NIP channel is complemented by the Near Infrared Spectrometer (NIS) and Visible Imager (VIS) described in companion papers.^{4,11} *Euclid*'s overall scientific aims, an overview of the mission and the translation to instrumental requirements are also available in this proceedings^{1,8} . It should be noted that after the *Euclid* assessment phase a new downscoped design was proposed by ESA in which the NIS and the NIP

instruments were merged into one single instrument (NISP) performing NIR photometry and spectroscopy. This paper will not refer to this new design proposal, but can be regarded as a baseline for further studies towards a final merged NISP design.

2. PRIMARY SCIENCE AIMS FOR PHOTOMETRY AND INSTRUMENT REQUIREMENTS

The weak lensing approach for cosmology requires at least a statistical knowledge of the distances, i.e. redshifts, of large numbers of individual galaxies. There are roughly 2.5 billion galaxies in the *Euclid* 2π survey area at a visible magnitude limit of $m_{AB} < 24.5$. Realistically this means that reliance must be made on photometrically estimated redshifts. To perform weak-lensing tomography the photometric information will be used to assign the measured galaxy sample to individual redshift bins. In a first step the shear signal is then extracted from the cross-correlation of the shape measurements of individual galaxies in different redshift bins. In a second step the statistical redshift distribution, $N(z)$, of the galaxies in a given bin is required to then map the results onto cosmological distance and thereby extract the cosmological information. The three near infrared bands (Y,J,H) provided by NIP can only be accessed from space and are required in this context to substantially reduce the number of catastrophic photo- z outliers as discussed in the *Euclid* Science Book.⁹ The requirement for the statistical error of the photometric redshift has been defined as $\frac{\sigma(z)}{1+z} = 0.05$ (goal: 0.03) in the range $0.2 < z < 2$. The science requirement for the photo- z precision has been broken down on instrument level. The final relative photometric accuracy (i.e. post-calibration) has been defined as $\delta F = dF/F < 0.005$. This requirement applies to the uniformity within a field and among areas on the sky. The final calibration includes the off-line data processing of the fields, which assumes additional ground based information (secondary standard stars) and the possibility of self calibration based on consistencies in the (redundant) *Euclid* data. The absolute photometric accuracy can be constructed from the high statistics within the *Euclid* data afterwards using standard stars. The error requirement on the mean of the redshift distribution $N(z)$ of each bin was found to be < 0.002 .

VIS and NIP share the same large 0.5 deg^2 FoV which is required to survey the entire extragalactic sky in the given mission duration of 4-5 years. The three NIP filters have been defined as Y(920-1146 nm), J(1146-1372 nm), H(1372-1600 nm (goal:2000)). This filter distribution provides the ideal synergy with ground based surveys. For each of the filters a limiting point source magnitude of 24 mAB (5σ) has been defined. The spatial resolution in the center of the J band (1259 nm) shall be between 0.3 and 0.36 arcsec (PSF FWHM) with a plate scale less or equal to 0.3 arcsec per pixel. The definition of the PSF sampling in the NIP aims to optimize the photometric result and is related to intra-pixel variations which become more important at lower PSF sampling. In the current design the PSF sampling requirement is approximately met (see 5.1) with a focal plane of 18 (3x6) H2RG detector arrays³ each with 2048x2048 pixels and a pixel size of 18 μm .

3. NIP CHANNEL DESCRIPTION

Euclid's optical concept is based on a Korsch-like $f/20$ three-mirror telescope. All three mirrors are pure conic and they are common to the VIS and NIP channels. After the third telescope mirror, at the pupil plane, a dichroic is located that separates the VIS and the NIP channel. At the dichroic the visible light is reflected towards the VIS channel while the near infrared beam is transmitted towards the NIP channel.

The NIP channel is a closed box interfacing on the Common Opto-Mechanical Assembly (COMA) that provides a common interface (I/F) structure for VIS and NIP (see Fig.1,2) towards the satellite payload module (P/L). The NIP optical bench consists of a sandwich element with a core made from an aluminum honey comb structure with Carbon Fiber Reinforced Plastic (CFRP) sheets. The mechanical loads are absorbed by the optical bench design. This optical bench supports the different subsystems:

- A Filter Wheel Assembly⁶ (FWA) with 3 NIR filters,
- A calibration source,⁷
- A four lens focal reducing optics turning the $f/20$ telescope beam into a $f/10$ instrument beam,

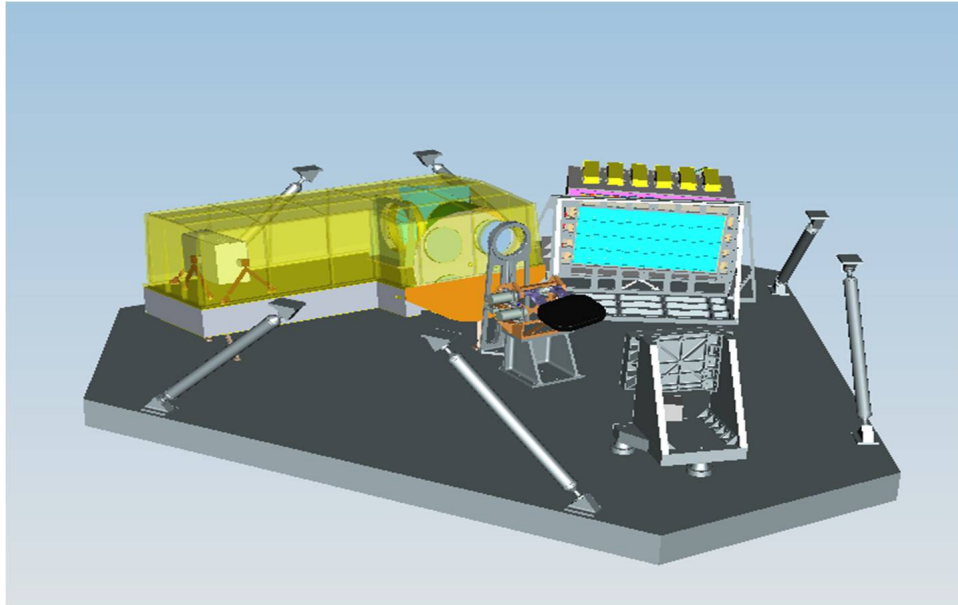


Figure 1. The NIP channel (left) and the VIS channel (right) mounted onto the COMA structure (grey).

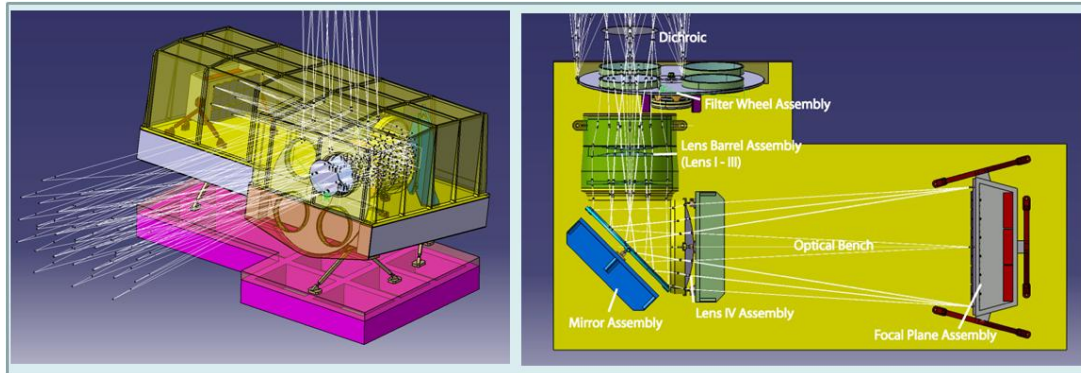


Figure 2. Left: The NIP channel with the closed cover (yellow) interfacing via bi-pods to the COMA (purple); Right: The main subcomponents of the NIP channel.

- A NIR Focal Plane Array (FPA) that consists of 3x6 Teledyne Hawaii 2RG (H2RG) detectors,³ with its application specific integrated circuit (ASIC) system, covering the 0.5 deg² NIR FoV,
- An additional control and compression electronics unit (CCU) is devoted to the processing of the NIP raw data while a dedicated power supply unit (PSU) converts the power from the primary power source to the NIP channel power requirements.

The optical bench is closed with a cover providing shielding against thermal loads and stray light.

The thermal and mechanical architecture of the instrument allows the structural elements to be passively cooled to 150 K operational temperature (to limit thermal radiation) and the NIR detectors (via a dedicated FPA radiator) to be at 100 K operational temperature (to limit dark current and detector cosmetics). These temperatures have been found to allow background (zodiacal light) limited infrared photodetection in all bands with a 2.5 μm cut-off filter. While the requirement on the upper cut-off wavelength of the H band was defined as 1600 nm (goal: 2000 nm), we nevertheless included the 2.5 μm cut-off case in our study to investigate its feasibility. Thermal passive cooling is ensured via thermal links from the instrument parts towards radiators

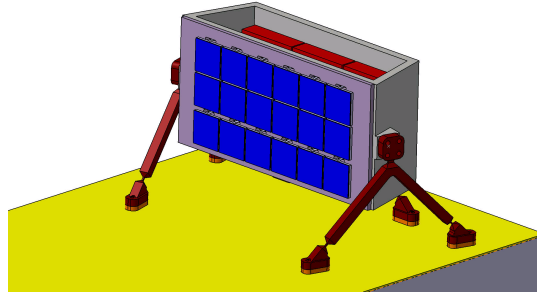


Figure 3. Illustration of the NIP FPA housing and bi-pod mount

located on the P/L. The NIP FPA (see Fig.3) is composed of 3x6 H2RG IR arrays (2048 x 2048 pixels each) (see Fig.7) with 18 μm pixels (2.5 micron cut-off) that cover the 0.5 deg² NIR FoV. To fill the gaps between individual detectors a four step dither pattern per FoV is required. The NIP channel will have the same dither pattern as the visible channel because dithering is achieved at spacecraft level. The FPA housing is a thermal mechanical structure that provides structural support of the massive focal plane array and ensures accurate location of the NIR detectors with respect to the IR image plane, and accurate location of the detectors with respect to each other. In addition it contains the cold read out electronics (considered baseline: 4 ASICs (2 nominal + 2 redundant) in 4 channel mode, alternative 18 ASICs + redundancy in 32 or 4 channel mode). The FPA housing is made of molybdenum with connecting bi-pods to the optical bench made from titanium. Its thermal functions are to ensure temperature stability of the assembly and to allow a thermal path to the power dissipated by the NIR detectors and ASIC electronics towards two separate radiators, one associated with the detector array and one with the NIP structure.

4. NIP INTERFACES

- Mechanical: The optical base plate of NIP is attached to the COMA structure via three (Inconel 718) bi-pods that allow accurate adjustment and thermal decoupling. The first hard mounted eigenfrequencies of the NIP on the COMA are driven by the design of the I/F pads and the mass distribution of the instrument. The current design requires an interface block (see Fig.2) below the NIP which is part of the COMA. A further iterative interface design by the EIC will lead to the suppression of the interface block and to the reduction of the bi-pods length that will lead to stiffer mounting and a lower mass of the assembly. This configuration could not be fully evaluated during the assessment phase but can be the reference of the next phase.
- Thermal: The NIP structure is thermally decoupled from the COMA structure and is thermally linked via thermal straps to a dedicated radiator located on the payload while a separate FPA radiator is thermally coupled to the detector array.
- Optical: The optical interface of the NIP channel is the dichroic. The dichroic, located on the COMA structure, reflects the visible wavebands and transmits the near infrared part of the observed light. At this position the input beam has an F-number of 20 and a beam diameter of ~ 130 mm.
- Electrical: Electronically the NIP CCU (associated to the channel but integrated on the P/L structure) interfaces to the PDHU⁵ (via space wire) and the payload mechanism control unit (PMCU) which is in charge of mechanism/thermal control and the control of the NIP and VIS calibration sources. In addition the PSU interfaces to the primary power control and distribution unit (PCDU) located on platform level.

5. OPTO-MECHANICAL DESIGN

The NIP optical system has been investigated under the assumption of a cold instrument (150 K) with a wavelength range of 900-2500 nm. These values have been chosen to demonstrate the feasibility of an increased

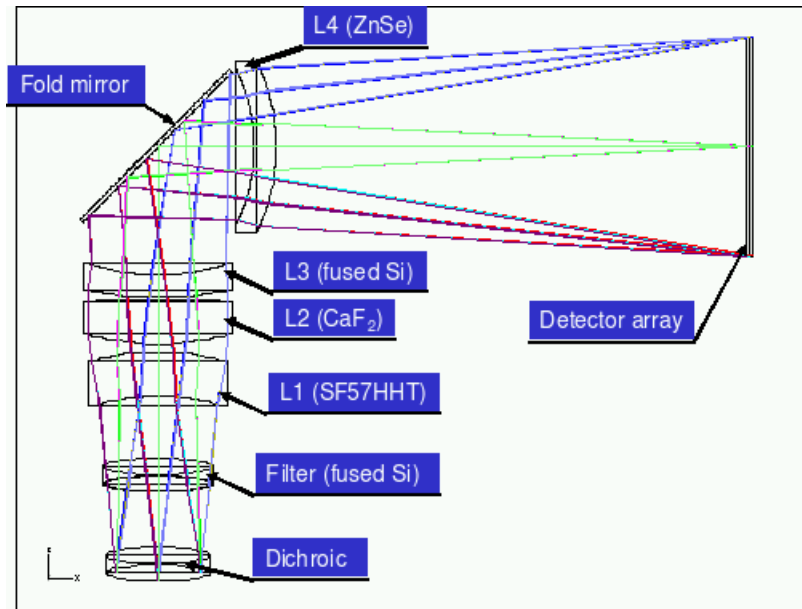


Figure 4. NIP Optical Design

filter cut-off of $2.5 \mu\text{m}$ and can be regarded as a worse case in terms of the required thermal boundary conditions.

Close to the dichroic element, near-infrared filters (coated fused silica or CaF_2) are placed near the exit pupil of the Korsch-type telescope. This position provides the smallest mechanical dimension of the filters, which is essential to guarantee good pupil image quality, low transmission loss, and smallest wave front error (WFE) contribution. The optical design of NIP is presented in Figure 4. The three bandpass filters are mounted in a filter wheel.⁶ Both, the dichroic and the bandpass filters are placed under a certain angle in order to avoid direct reflections causing ghosts on the detectors. The substrate material of the bandpass filters is fused silica, which has good mechanical and optical properties. In the NIP channel's wavelength range it is insensitive to cosmic radiation. Beside the filters, the on-axis optical design of the NIP channel consists of a 4 lenses (SF57HHT, CaF_2 , Fused silica, ZnSe) focal reducer turning the $f/20$ telescope beam into a $f/10$ instrument beam. The maximum thickness of a single lens is 50 mm (L1) and the maximum diameter is 179 mm (L4). The total mass of the lenses is 12.5 kg. An additional fold mirror intersects the focal reducer after its third lens to reduce the mechanical size of the instrument. The first 3 lenses of the focal reducer are installed in a lens barrel made of titanium to adapt the coefficient of thermal expansion (CTE) to the average CTE of the lens package. The barrel itself is attached to three bi-pods (material aluminum or Inconel). This mounting concept is considered feasible because of a very low thermal gradient at operation temperature. With NIR anti reflection coatings on both lens sides the overall optical transmission is expected to be $> 80 \%$. The lens radii and the distances between the lenses have been chosen such that there are no focused reflections from the lens surfaces into the detector. The lens design provides diffraction limited image quality at the specified wavelengths. Degradation of the PSF due to manufacturing and alignment tolerances, as well as thermal changes are expected within an acceptable range. The fold mirror is made of gold-coated-fused silica with titanium support interface in order to have a similar CTE as the optical base plate. The mounting of the mirror frame to the bracket will be done with three clamps, which are fixed on the bracket with screws on one side and hold the mirror frame with clips on the other. The bolt between is tapered in the middle to minimize the heat flux.

5.1 Optical performance

The result of the optical performance assessment, which has considered the current mechanical, structural, and thermal design of the instrument, demonstrates the excellent optical and mechanical performance of the NIP photometer design.

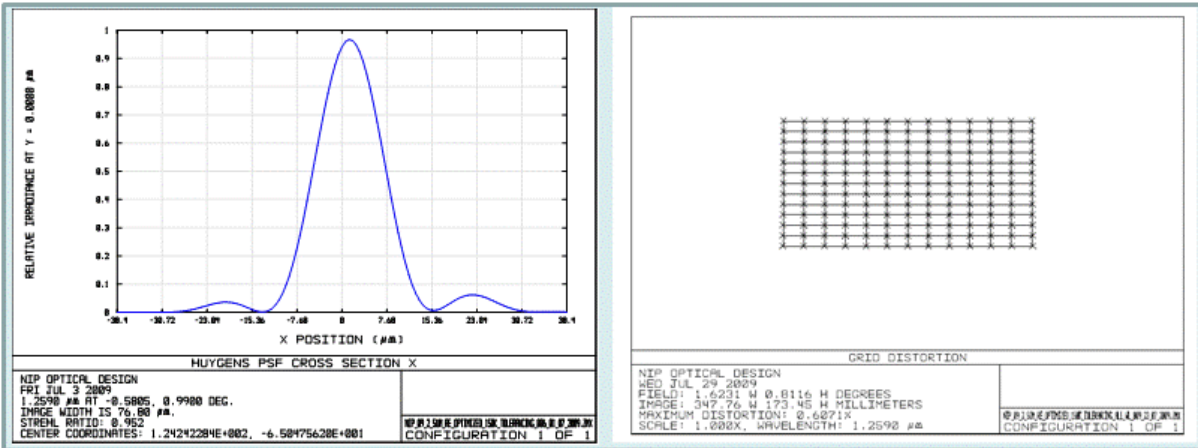


Figure 5. (left) Monochromatic PSF of NIP + telescope configuration at the largest field angle calculated at 1259 nm, (right) Grid distortion of the NIP optics

In the following we list the main conclusions from the optical performance analysis. The NIP optical reference design was provided by ESA. This design was optimized for ambient temperature and pressure operation; therefore, a re-optimization of the design for 150 K operating temperature has been performed up to a wavelength of 2.5 μm . We conclude that the performance of the optics after optimization remains diffraction limited and comparable with that of the ESA design. The RMS WFE has been investigated as a function of wavelength and position within the FoV. It was found that over the desired spectral and spatial range the wavefront error of the optical system is well within the diffraction limit.

The performance of the optical system can be characterized by the Strehl number. Diffraction limited performance is characterized by a Strehl number of > 0.8 while the calculated Strehl number is > 0.9 , which demonstrates the good optical quality of the design. The FWHM dimension of the PSF is $< 13 \mu\text{m}$ for all configurations (FWHM = 12.9 μm (center FoV) and 12.8 μm (edge FoV) @ 1259 nm). The photometer provides low distortion images ($< 1\%$) in the required wavelength range (see Fig.5).

The FWHM of the current nominal PSF ($< 13 \mu\text{m}$) is less than the detector pixel size of 18 μm . In this case the detector Pixel Response Function (PRF) may lead to a degradation of the photometric performance due to intra pixel variations. For this reason we investigated whether the scientific requirements are met or if an enlargement (e.g. via a dithering mirror) of the PSF FWHM is required.

Inter Pixel Capacity (IPC), lateral charge diffusion, optical cross talk and intra pixel variations contribute to the pixel response function (PRF). The PRF has been measured for the H2RG 1.7 μm cut-off detector by N. Barron et al.² Based on this data and assuming a similar PRF (one dimensional) for the 1.7 and 2.5 μm detectors the impact of the PSF FWHM on the photometric accuracy has been investigated. It can be concluded that the actual size of the PSF FWHM is not expected to be critical with respect to the photometric calibration requirements. Due to the dithering strategy the subexposures per FoV are sufficient to reduce (averaging out) the photometric error caused by the detector effects to a level which is well acceptable and in line with the photometric requirements. Nevertheless additional detector tests are required to confirm the PRF performance of the 2.5 μm detectors.

5.2 Optical Tolerance and Load Case Analysis

The operating temperature of the instrument structure was set to 150 K. At this temperature a tolerance analysis has been carried out and the performance has been verified using Monte Carlo simulations. The tolerance analysis shows that the L4 lens in the focal reducer requires tight tolerances regarding element decenter and tilt. Therefore, these two parameters have to be monitored during the assembly procedure of the optics. The performed Monte Carlo simulation (with 2000 models) describes the statistical behavior of the manufactured and aligned system.

It can be concluded that the applied manufacturing and alignment tolerances promise very good, diffraction limited performance at high confidence level.

In addition we performed an optical performance check for two load cases:

- 1 g gravity release
- Thermo Elastic Load Case: Thermo-Elastic due to variation of operational temperatures in the range of +/-2 degrees

In order to support this check a detailed thermo-mechanical Finite Element Model (FEM) analysis has been performed (using ESATAN TMS r1 and NASTRAN) in order to simulate the mechanical and thermal performance of the NIP channel (see Fig.6). The displacements (translations and rotations) of the optical elements due to the above mentioned load cases were then investigated with the Zemax optical design software.

The system performance concerning gravity release is well within the specified PSF budget of the system. The impact of position changes of the optical elements on the optical performance is marginal with respect to the PSF dimension. The impact of all optical surface deformations on the optical performance has to be analyzed in the next phase in order to confirm all effects of the gravity release.

Thermal flows introduced by the satellite and instrument might impact the NIP channels opto-mechanical structure and could degrade its optical performance via thermal gradients and their related mechanical deformations. Therefore, in a first step, an overall optical temperature sensitivity analysis has been performed using Zemax. The derived tolerance for the temperature range was +/- 2K for the optical system. Within this temperature range the instrument performance stays within the diffraction limit. In an iterative process the thermo-mechanical design of NIP was optimized to fulfill this requirement.

To achieve a more realistic picture of the optical performance under consideration of thermo-mechanical deformations (within the +/- 2K temperature range) the thermo-mechanical finite element model of NIP has been used. Using this model the thermo-mechanical deformations of the instrument (under operational conditions) have been precisely characterized. The changes in position and orientation of the optical elements were finally imported into Zemax. It can be concluded that the PSF FWHM and the Strehl ratio are sufficiently stable within the +/-2 K temperature range. Therefore, this range can be the baseline for the thermal design of the instrument.

6. THERMO-MECHANICAL ANALYSIS

Photometric and detector noise evaluations show that a NIP FPA temperature of 100 K and a NIP instrument temperature of 150 K is sufficient to reduce the detector dark current (~ 0.1 e/s/pixel) (with 2.5 μm cut-off detectors) and the thermal radiation of the instrument to achieve background limited infrared photodetection in all filters, with the filter cut-off extended to 2.5 μm at the longest wavelength (assuming the telescope to be at ~ 200 K leading to a background contribution of 10 % of the zodiacal background).

The baseline assumptions that were considered in the thermo-mechanical analysis were:

- NIP channel hard mounted via 3 bi-pods to the COMA
- COMA I/F temperature of 200 K (worse case assumption)
- Instrument Electronic BUS temperature of 293 K (TBC)
- Power consumption: Filter wheel: ~ 0.04 W (time average), FPA: ~ 3.6 W (32 channel mode at 100 kHz, considered as worse case)
- Instrument at ~ 150 K (optics: +/- 2 K) , detectors at 90 K (+/- 0.5 K), 120 K worse case.
- ASICs temperature < 200 K (+/- 1 K)

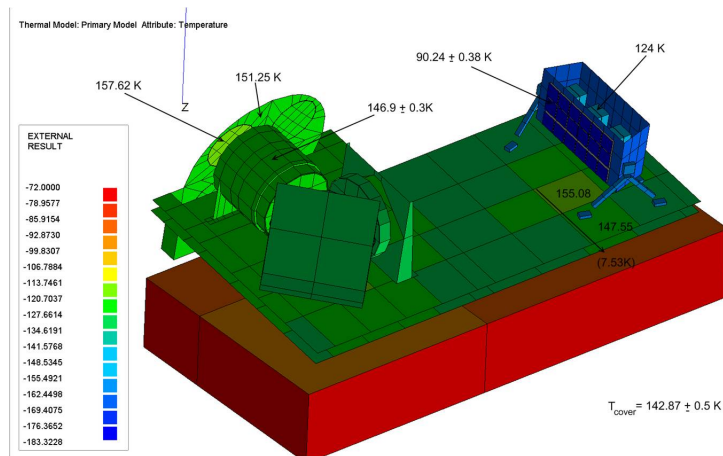


Figure 6. Thermal FEM model of the NIP channel showing the temperature distribution over the instrument (under operational conditions).

6.1 Mechanical Analysis

A structural analysis of the design has been achieved based on a NASTRAN Finite Elements Model (FEM) with its main components: the FPA-Unit, the lens 4 fixation, the fold mirror, the barrel with 3 lenses and a filter wheel assembly (note that the FWA was an early preliminary design, and that a more detailed design has been investigated⁷). The model is suitable for evaluation of deformations, stresses, fundamental eigenfrequencies, mode shapes and effective masses of the instrument. The cover was assumed to provide no mechanical stiffness.

Outputs of this analysis are used for the NIP optical design assessment presented in 5.2. The main outcomes of the structural analysis are: The first fundamental eigenfrequency of the NIP channel is at 131 Hz. The lowest eigenfrequency for a single part is at 73 Hz from filter wheel motions. A modification of the filter wheel should provide an eigenfrequency above 100 Hz for the complete FWA. The calculated margins of safety for the structural parts (with design load factor 80 g) are positive except for the bi-pods to COMA interface and the bi-pods to FPA housing interface. In further phases of the project an improved design and detailed modelling of the bi-pods is necessary as well as a confirmation for the applicable maximum design load factor. The stresses induced by the temperature difference between integration and operational conditions can be sustained with positive margins of safety. From a structural point of view the design is robust with the two exceptions as stated above.

6.2 Thermal Analysis

A thermal analysis of the proposed design has been performed in order to check the feasibility of passive cooling for the required temperatures (instrument and FPA) with reasonable radiator size and to model the thermal impact on the optical performance (see 5.2). The main philosophy of the thermal design is to provide a thermal path to remove the generated and induced heat loads and to thermally isolate the dissipating parts. Based on the previous thermal-mechanical design, a Finite Element Model analysis of the thermal behavior of the NIP channel has been computed. In the thermal model the outer surfaces of the structure were assumed to be covered with Multi Layer Insulation foil (MLI) while the internal surfaces were assumed black for stray light reduction. The COMA I/F was modeled as a thermal boundary box while the radiators and cooling straps were not geometrically modeled. The optical bench was modeled as a CFRP-honey comb composite and the lenses were modeled with their respective geometrical thickness.

The analysis shows that the required radiator sizes depend mainly on:

- SAT I/F temperature (radiative and conductive heat transfer)
- Cable connection between ASICs , H2RGs and COMA electronic BUS

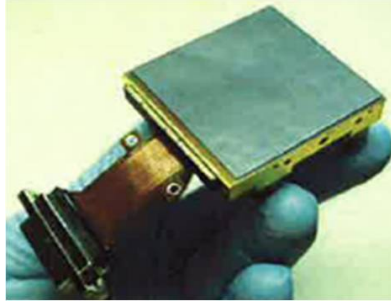


Figure 7. The Teledyne H2RG detector.³

- Readout frequency and channel mode (FPA power dissipation)

We found the following total radiator sizes (FPA + instrument radiator) as a function of the required detector temperature and COMA I/F temperature.

	COMA at 150 K	COMA at 200 K
Detectors at 90 K	$\sim 1 \text{ m}^2$	$\sim 1.6 \text{ m}^2$
Detectors at 120 K	$\sim 0.25 \text{ m}^2$	$\sim 1.25 \text{ m}^2$

Table 1. Total radiator sizes (FPA + instrument radiator).

At the end of the assessment phase the COMA temperature was set to 150 K, this relaxes the constraints on the NIP radiator sizes. The simulation assumed the 32 channel read out mode and its related power consumption. Switching to a 4 channel read out mode may further relax the constraints on the NIP radiators. The temperature gradients of the detector arrays were found to be within their specified range of +/- 0.5 K for detector temperatures between 90K and 120 K.

7. FOCAL PLANE ARRAY ASSESSMENT, DETECTOR READOUT AND SENSITIVITY

The NIR Focal Plane Array is composed of the following elements:

- 3x6 Teledyne Hawaii 2RG IR arrays detectors with 18 μm pixel pitch
- 4 ASICs as readout electronics (2 nominal (8 H2RGs per ASIC) + 2 redundant) / alternative: 18 ASICs (1 H2RG per ASIC)
- FPA housing made of molybdenum with connecting bi-pods (titanium) interfacing towards the NIP optical bench

The Teledyne H2RG array has been selected for the *Euclid* NIP channel due to its high technical readiness level (TRL) and compliance to the detection requirements of the mission. A trade-off analysis has been performed concerning the cut-off wavelength of the H2RG detectors with 3 options considered: 1.7, 2.0 and 2.5 μm cut-off. While all three detectors achieve similar quantum efficiency (85-90 %), the dark current increases as the cutoff wavelength increases, requiring the 2.0 and 2.5 μm cut-off detectors to operate at cooler temperature in order to reach the required dark current specifications. It has been demonstrated that the 2.5 μm cut-off detector has a lower read noise than the 1.7 μm cut-off detector, however, with non-destructive readout sampling, the required readout noise can be achieved with both. The H2RG 2.5 μm cut-off detectors have a higher TRL than either the 1.7 or 2.0 μm detectors. Based on TRL level, Teledyne experience and expected science gain, the EIC baseline detector is the Teledyne 2.5 μm cut-off H2RG detector.

Photometric calculations show that the zodiacal background in each of the filter is not higher than ~ 0.4 e-/s/pixel (at ecliptic pole). To achieve background limited observations a 25 % criterion for the dark current is

sufficient. Therefore the detector dark current should be < 0.1 e-/s/pixel. Based on information supplied by the manufacturer this requires an operational temperature of ~ 100 K for the baseline detector.

H2RG detectors have the option of 1, 4, or 32-channel outputs. The analog-to-digital conversion is performed by the ASIC electronics provided by Teledyne. The 18 H2RG arrays are connected via a custom flex harness to 2 ASIC chips mounted inside the FPA housing close to the arrays. The main task of the ASIC electronics is detector readout and analog-digital conversion. The current concept for the EIC uses the 4-channel output option at 200kHz. The 4-channel output, which provides a lower frame-rate, was selected to decrease in power consumption, required number of ASICs, required computing power, the thermal considerations associated and costs. The reduction of read-out noise is achieved by following a sampling up-the-ramp read out strategy. Sampling up-the-ramp has the advantage to allow saturation detection and glitch detection while it decreases the effective read noise by $1/\sqrt{\frac{N}{6} \cdot \frac{(N+1)}{N-1}}$. Within the current observing scheme (i.e. 140 s integration per dithered image, 4 channel read out mode, 200 kHz read out frequency) we achieve $N \sim 26$ non destructive read outs leading to a 6 e- rms noise for a 2.5 μm cut-off detector with sampling up-the-ramp (assuming single CDS noise of 13 e-).

Using an exposure time calculator, it has been demonstrated that with the proposed read out scheme the required signal to noise can be achieved in: 82s in the Y-band, 111s in the J-band and 61s in the H-band (integration time per sub-exposure (1 out of 4 per FoV)). The overall NIP integration time is uncritical since the required VIS channel integration time is ~ 450 s per sub-exposure. Therefore the VIS channel is the driver for the total integration time.

An assessment concerning the detector saturation, non-linearity, radiation hardness and persistence has been performed. In the following we list the main conclusions: It was found that less than 0.025 % of the total pixels will be saturated by near-field stars during a 140s integration time. The expected average linearity for the H2RG detectors is < 2 %. It is possible to measure the linearity variation from pixel-to-pixel, and if done, calibration and correction should be possible, but needs to be further explored. JPL has developed a technique to extract the imager average conversion gain from CMOS FPAs, which has been applied to InGaAs FPAs, but not yet applied for HgCdTe FPAs. For accurate photometry, we will need to develop pixel-level test methodology and correction algorithms (i.e. determine the cause of flat field variations at required photometric accuracy limit). The H2RG (2.5 μm cut-off) detector has been tested to meet the requirements of the James Webb Telescope (JWST), which will also operate at L2. The detector was shown to reach TRL6 and continue to function after encountering more than the expected lifetime Total Ionizing Dose (TID) while unshielded. These tests were performed at 37K and the H2RG detectors were demonstrated to endure TID=20 krad. Additional radiation tests under the NIP operational conditions may be required. For every pixel illuminated by a near-field star or a lensed galaxy during the 140s integration time in a given band and sub-exposure, 0.23 % of the initial signal will persist into the following frame (i.e. dither position). This persistence was measured¹⁰ on the 1.7 μm cut-off detector. The latent images due to initial images of lensed galaxies are negligible because the initial signal is small. For near-field bright stars, using a star population model,¹² we estimate an upper limit per band of total pixels illuminated by bright stars in the first frame to be < 0.2 %, and the latent images due to those stars in the following frame to be < 0.01 % of the total FPA. The probability of a lensed galaxy image coinciding with either an image or latent image of a near-field star is negligible (< 0.001 %).

8. ELECTRONIC DESIGN

The result of the electrical study is a proposed baseline instrument interface electronics concept, whose principal feasibility in terms of instrument performance and technical implementation has been successfully demonstrated. In the following we summarize the main results.

8.1 Functional Architecture

The NIP channel electronics architecture encompasses the following three main elements: the H2RG detectors, the SIDECAR ASICs and the Control and Compression Unit (CCU). The CCU is composed of the following sub-units:

- A Data Processing Unit (DPU) for slope generation, glitch detection and substitution, saturation detection and the data transmission towards the PDHU. The DPU is the hardware on which the required data processing is realized and formatting of the digital data stream down to the output of a CCSDS formatted data stream to the PDHU. This includes the pre-processing of all digital data from the SIDECAR ASICs. The DPU also includes a clock generator.
- A NIP Instrument Control Unit (ICU) which includes the control electronics for SIDECAR ASICs (configuration and monitoring) and the control electronics for temperature control of the detectors and SIDECAR ASICs. The ICU consists of a processor module connected to the PDHU via space wire I/F and controls all sub-units within the NIP. The baseline is to have this unit integrated into the PMCU. It is responsible for collection of housekeeping data including temperatures, analogue values, bi-level status signals etc. The ICU also receives the on-board time (OBT) from the PDHU and correlates the ICU time with the clock used in the DPU for time stamp of the user data. The ICU will also receive synchronization information regarding the instrument imaging sequence from the PDHU.
- A Power Supply Unit (PSU) that consists of DC/DC converters and provides all the necessary supply voltages for the NIP internal functions and modules, and also includes the galvanic isolation to the unregulated 28 V main bus.

All subsystems need to provide redundancy in order to guarantee reasonable reliability figures.

8.2 On Board Data Processing

In the current baseline an image is built by 140-s integration time on the 18 HAWAII-2RG detectors each having 2048 x 2048 pixels digitized to 16 bits values. This results in 1.2 Gbits / frame to process. The H2RG arrays are planned to be operated in the 4 channel readout mode at 200 kHz readout frequency resulting in a time to generate a frame of 5.25 s. The 18 detectors with 4 read-out channels each generate 72 output signals feeding the 2 SIDECAR ASICs (36 input data channel each). 26 frames are generated over an image integration time leading to 31 Gbits of data delivered at a 230 Mbps rate to the DPU input during the 140 s of an image integration time. The time span available for the DPU to process the received detector data is approximately 140 s and to transmit the results to the Payload Data Handling Unit (PDHU) is 10 s. The NIP instrument has a processing requirement of about 105 MOPS per second, a constant input data rate of 230 Mbps (during the integration time), a constant output data rate of 121 Mbps (in the following 10 s at the end of the integration time) and an intermediate memory with 15 Gbit capacity (including storage of the EDAC information). The above estimate ignores all overhead processing, processor wait states, bus and memory bandwidth limitation. It is also assumed that data is available in the order of processing. Considering the data processing and the memory requirements of the DPU, about 2 modules would be required to implement this functionality. Each module essentially consists of one data processing device and the necessary peripherals, offers processing capabilities, memory storage for intermediate data and broader communication interfaces, which are required to implement the data processing. The module also consists of signal conditioning logic for the incoming and outgoing data signals. On the input side the data processing module is connected with the SIDECAR ASICs and on the output side it is connected with PDHU via SpW interface. Currently it is assumed that the processing device interfaces with up to two external memory banks. The external memories are EDAC protected on-the-fly and no timing penalty occurs during correction. The recommended EDAC algorithm detects and corrects a single bit error in a 32-bit word and detects a double bits error in a 32-bit word. Any error correction and/or detection are recorded by the memory interface and can be included in the house-keeping information. A configuration memory is needed on the data processor module to store the configuration data in case an array processor or SRAM-based FPGA solution is chosen. The contents of the configuration memory are EDAC protected.

8.3 Processor Architectures

A requirement of about 105 MOPS of processing power is assumed here. A quantitative comparison of different processing architectures has been investigated taking into account the following technology: DSPs, PowerPCs, Array Processors, ASICs, SRAM-based FPGAs and Anti-fuse FPGAs. From a trade-off analysis the recommended solution is the use of an Anti-fuse FPGA. As a fall back solution, the Array Processor is recommended.

Although currently not necessary, this gave the additional opportunity of changing the computation very late in the project, even during flight, as its functionality can be changed by uploading of a new software configuration.

The required processor architecture depends strongly on the assumption on: the read out scheme, number and definition of algorithms to be performed, number of detectors. Also if no major problems for the electronics related to the current NIP baseline assumptions have been identified, a fine trade off between the mentioned assumptions and the electronics hardware must be performed for optimization.

9. TOTAL POWER AND MASS BUDGET

A total power consumption of 31 W has been evaluated for the NIP interface electronics unit. This figure is independent of the redundancy scheme chosen for the unit as all the modules are operating in a cold redundant configuration. The total mass of the NIP channel has been calculated as ~ 80 kg (without any mass optimization during the assessment study and without margins) excluding the electronics. The mass of the electronics has been estimated as ~ 12 kg including the redundant electronics part.

10. CONCLUSION AND STEPS FORWARD

The EIC assessment study of NIP has demonstrated the overall feasibility and good performance of the proposed NIP instrument concept, no show stoppers have been identified. At the same time we have identified further room for optimization: i.e. the design of a stiffer NIP and FPA mounting concept, re-design of the FWA mounting concept to increase its lowest fundamental eigenfrequency, final trade-off between required electronics hardware and the required processing algorithms and the baseline FPA read-out concept, mass optimization. In addition further studies must be performed to investigate the PRF performance of the $2.5 \mu\text{m}$ detector.

11. ACKNOWLEDGMENTS

For their substantial contributions we would like to thank: DLR, ESA, Kayser-Threde GmbH, Teledyne Technologies Inc and the *Euclid* Imaging Consortium. The technical studies have been supported by DLR under BMWT grant 50 OD 0803

REFERENCES

- [1] Amiaux, J. et al., "Euclid imaging channels: from science to system requirements", these proceedings, SPIE(2010)
- [2] Barron, N. et al., "Sub-Pixel Response Measurement of Near-Infrared Sensors", PASP,119:466-475 (2007)
- [3] Beletic, J.W. et al., "Teledyne Imaging Sensors: infrared imaging technologies for astronomy and civil space", SPIE 7021 (2008)
- [4] Cropper, M. et al., "VIS: the visible imager for *Euclid*", these proceedings, SPIE(2010)
- [5] di Giorgio, A. et al., "The data handling unit of the *Euclid* imaging channels: from the observational requirements to the unit architecture", these proceedings, SPIE(2010)
- [6] Holmes, R. et al., "The Filter Wheel Mechanism for the *Euclid* Near-Infrared Imaging Photometer", these proceedings, SPIE(2010)
- [7] Holmes, R. et al., "The *Euclid* Near-Infrared Calibration Source", these proceedings, SPIE(2010)
- [8] Laureijs, R. et al., "The *Euclid* Mission", these proceedings, SPIE(2010)
- [9] Refregier, A. et al., "Euclid Imaging Consortium Science Book", ArXiv e-prints (Jan. 2010)
- [10] Smith, R. et al., IEEE Nuclear Science Symposium Conference Record, (2007): 2236-2245
- [11] Valenziano, L. et al., "The E-NIS instrument on-board the *Euclid* Dark Energy Mission: a general view", these proceedings, SPIE(2010)
- [12] (<http://model.obs-besancon.fr/>)